LIMNOLOGY
and
OCEANOGRAPHY: METHODS

ASLO

Limnol. Oceanogr.: Methods 21, 2023, 718–733

doi: 10.1002/lom3.10577

The ZooScan and the ZooCAM zooplankton imaging systems are intercomparable: A benchmark on the Bay of Biscay zooplankton

Nina Grandremy,[1]* **Christine Dupuy**,[2] **Pierre Petitgas**,[3] **Sophie Le Mestre**,[4] **Paul Bourriau**,[1] **Antoine Nowaczyk**,[5] **Bertrand Forest**,[6] **Jean-Baptiste Romagnan**[1]*

[1]DECOD (Ecosystem Dynamics and Sustainability), IFREMER, INRAE, Institut Agro, Centre Atlantique, Rue de l'Ile d'Yeu - BP 21105, Nantes, 44311, France
[2]BIOFEEL, UMRi LIENSs, La Rochelle Université/CNRS, La Rochelle, France
[3]IFREMER, RBE, Centre Atlantique, Rue de l'Ile d'Yeu, Nantes, France
[4]DECOD (Ecosystem Dynamics and Sustainability), IFREMER, INRAE, Institut Agro, Plouzané, France
[5]UMR CNRS 5805 EPOC–OASU, Station Marine d'Arcachon, Université de Bordeaux, Arcachon, France
[6]IFREMER, RDT-LHYMAR, Centre Bretagne-ZI de la Pointe du Diable, Plouzané, France

ABSTRACT

Zooplankton analysis represents a bottleneck in marine ecology studies due to the difficulty to obtain zooplankton data. The last decades have seen the intense development of zooplankton imaging systems, to increase the zooplankton data spatio-temporal resolution as well as enabling the combination of size, taxonomy, and functional traits in aquatic ecology studies. Here, we propose a benchmark between the ZooScan, a commercially available, laboratory-based scanner, which analyses zooplankton preserved samples, and the ZooCAM, an in-flow imaging system designed for on-board live zooplankton imaging. Sixty-one zooplankton samples collected over the Bay of Biscay in environments ranging from estuarine to offshore blue waters were imaged with both instruments. Zooplankton Normalized Biovolume-Size Spectra slopes, mean sizes, abundances, and zooplankton community biogeographical patterns were computed for each instrument and compared at the taxonomic group, the sampling stations and the Bay of Biscay scales. Both instruments produced similar zooplankton variables by stations and by taxa and described similar zooplankton community compositions and biogeographical patterns, on the large mesozooplankton size range, i.e., [0.3–3.39] mm ESD. We conclude that the ZooCAM and the ZooScan data can be combined to generate long term or spatially resolved zooplankton time series. Our study shows that benchmarking imaging instruments or techniques (1) offers a robust assessment of interoperability between instruments, mitigating possible instrumental biases, and (2) may be of great interest in the case of instrumental obsolescence or breakdown, to choose the most conservative replacement solution in a long term time series framework.

Metazoan zooplankton (hereafter referred to as zooplankton) is a key biological compartment in marine ecosystems. Knowledge on their spatial distribution patterns and communities' composition at regional and global scales over time is critical to address overall ecosystem health and biodiversity conservation policies (Chiba et al. 2018; Batten et al. 2019), and predict

*Correspondence: grandremy.n@gmail.com; jean.baptiste.romagnan@ifremer.fr

Author Contribution Statement: B.F. is involved in the ZooCAM maintenance and developed the ZooCAM software. J.B.R., S.L.M., and P.B. were involved in the zooplankton samples collection and imaging with the ZooCAM during the PELGAS survey in 2016. N.G. digitized the samples with the ZooScan. J.B.R., N.G., and A.N. scrutinized and identified the organisms vignettes. J.B.R. and N.G. performed the data computation and analyses, and wrote the manuscript. All the co-authors reviewed the manuscript and agreed with the content of the final submitted version. All the co-authors made a significant contribution to this work.

Additional Supporting Information may be found in the online version of this article.

marine ecosystems and climate dynamics (Hofmann 2010; Mitra and Davis 2010). These organisms have a central position in the food webs, transferring the matter and energy from the primary production to higher trophic levels such as commercially and ecologically important pelagic fish species (van der Lingen 2002; Beaugrand et al. 2003). Because of their short generation time, they are sensitive to environmental changes and therefore can be used as good climate change indicators (Hays et al. 2005; Beaugrand et al. 2015). In addition, zooplankton play important roles in global biogeochemical cycles (Banse 1995), participate in the oceanic mitigation of atmospheric CO_2 build up through active processes, e.g., grazing and vertical diel migration, and passive processes, e.g., repackaging of fast sinking fecal pellets (Ariza et al. 2015; Turner 2015; Stukel et al. 2022). Given these key functions, abundance, biomass, and diversity of zooplankton are now considered as essential ocean variables and essential biodiversity variables (Chiba et al. 2018; Batten et al. 2019; Lombard et al. 2019).

Despite this recognized importance, general description and understanding of zooplankton communities often remain fragmented in space and time. The traditional zooplankton data collection is based on vertical net hauls and preserved samples examination under binocular microscope by trained taxonomists (UNESCO 1968). This analysis protocol enable a detailed identification level of organisms suitable for biodiversity-based studies, single sampling point time series, or one shot studies. However, this is a time-consuming, labor-intensive, costly, and error-prone process. Counting and sorting planktonic organisms under a microscope during long periods can lead to fatigue of the operator (Culverhouse et al. 2014; Pitois et al. 2018) and end up in inconsistencies in both counting and classification, resulting in non-repeatable outputs. In addition, the number of taxonomic experts has declined over the last 50 yr leading to an increased lack of zooplankton taxonomy skills (Culverhouse 2015; Pitois et al. 2018). We consider that this traditional zooplankton data acquisition process, as useful and relevant as it is, is becoming increasingly less sustainable in the context of accelerating science, increasing scarcity of trained experts, and increasing competition for funding.

On the other hand, numerous zooplankton imaging systems were developed during the last two decades encompassing laboratory-based, on-board and in situ instruments. These newly developed imaging instruments rely on different imaging sensors and techniques such as commercially available digital cameras, flatbed scanners, linescan camera or holographic camera, e.g., and could be based on different imaging methods such as steady imaging, in-flow imaging, or shadow imaging. These imaging instruments also differ in their image resolutions, sampled volumes, organisms' size range target, and whether they are able to image live organisms, preserved samples, or both. In-depth reviews of zooplankton imaging instruments conditions of use, specifications and capabilities can be found in Lombard et al. (2019) and Romagnan et al. (2016).

Modern imaging instruments often generate thousands to millions individual images of precisely sized organisms and particles per dataset. Consequently, they are often associated with semi- or fully automatized image classification tools based on machine-learning to accelerate the examination and taxonomic identification steps and decrease the expert intervention time (Benfield et al. 2007; Irisson et al. 2022; Rubbens et al. 2023). However, imaging-based zooplankton data are not as taxonomically detailed as what is humanly possible with traditional binocular analysis, and often require post-processing validation and correction, and category aggregation to produce scientifically usable data (Luo et al. 2018; Irisson et al. 2022). Yet, zooplankton imaging associated to machine-learning increased the feasibility of size-based and functional groups studies, and more recently of trait-based approaches to zooplankton ecology (Orenstein et al. 2022) as well as improved the reconstruction of long time series by enabling the integration of non-analyzed samples from the past in on-going series (see Irisson et al. 2022 for a thorough review of the combination of zooplankton imaging and machine-learning). Finally, the use of commercially available instruments producing standardized datasets is favorable to collaborative work between institutions (Gorsky et al. 2010). Zooplankton imaging is now considered a robust and cost effective approach to large-scale studies, long time series reconstruction and monitoring, in order to improve zooplankton ecology knowledge (Lombard et al. 2019).

However, the variety of zooplankton image collection methods and techniques, and achieved taxonomic resolution may make it difficult to compare, aggregate, and analyze zooplankton datasets originating from different imaging sources. Comparison studies between instruments are highly needed to assess the agreements and discrepancies in the results obtained from different instruments, and provide information on their interoperability (e.g., Pitois et al. 2018; Naito et al. 2019; Whitmore et al. 2019) to envision the incorporation of zooplankton into global ocean observing systems (Lombard et al. 2019).

The aim of this study is to assess in detail the interoperability of two imaging instruments: the ZooScan and the ZooCAM. Both instruments are used for the analysis of net collected zooplankton samples. The ZooScan is a commercially available, laboratory-based, waterproof scanning system used to generate high resolution zooplankton images from preserved samples (Gorsky et al. 2010). It is now widely used worldwide. The ZooCAM is a benchtop in-flow instrument developed to image live, net collected, zooplankton samples, on-board (Colas et al. 2018). It is used during the PELagic GAScogne (PELGAS) cruise in the Bay of Biscay for imaging spatially resolved zooplankton and fish eggs samples since 2016 (Doray et al. 2018). The zooplankton samples collected during PELGAS before 2016 were preserved and subsequently analyzed at the

lab with the ZooScan. The extension of the historical PELGAS zooplankton time series with recent (and on-going) ZooCAM data thus depends on the interoperability of the two instruments. A preliminary study showed that both instruments output to similar zooplankton communities' compositions, total abundances and size spectra slopes using nine samples collected in shallow coastal area (Iroise Sea) in the Northern Bay of Biscay (Colas et al. 2018). The reduced number of samples and the homogeneity of the sampling location do not totally exclude uncertainties on the interoperability of the two instruments for samples originating from more hydrologically diverse environments. Here, we compare the taxonomic composition, size structure and spatial patterns of the zooplankton community obtained with the ZooScan and the ZooCAM over the whole Bay of Biscay continental shelf, encompassing deep oceanic waters, stratified shelf waters and coastal seascapes (Petitgas et al. 2018). We hypothesize that despite their set up difference, the two instruments would provide similar zooplankton community descriptors, for a wide variety of habitats from coastal to offshore, and eutrophic to oligotrophic environments (Fig. 1). If this hypothesis is validated, the ZooCAM would enable the extension and continuation of the ongoing zooplankton PELGAS time series, and could be an on-board alternative to land based ZooScan imaging work.

Materials and procedures

Samples collection

Zooplankton samples were collected during the PELGAS2016 integrated survey (Doray et al. 2018) that was carried out over the Bay of Biscay French continental shelf, in spring 2016 on board the R/V "Thalassa". Zooplankton samples were collected at 61 stations (Fig. 1) during night time with a 200-μm mesh size WP2 net vertically towed from 100 m (or 5 m above the seabed) to the surface. The net was fitted with a flowmeter (Hydrobios) to measure the sampled water volume. The samples were collected in habitats ranging from shallow, coastal, tidally mixed, and eutrophic waters to > 500 m deep, offshore, stratified, and oligotrophic waters.

Samples imaging with the ZooCAM

The samples were analyzed live on-board during the survey with the ZooCAM. The ZooCAM is an in-flow imaging instrument (pixel size: 10.3 μm), allowing the immediate imaging of samples after collection (Colas et al. 2018). Prior digitization, the zooplankton samples were subsampled with a Motoda splitter, to reduce the density of objects to be analyzed, along with the risk of imaging overlapping objects. The Motoda splitter enable a dichotomic partitioning of samples. The first step partitions the sample in two halves. The subsampling ratio is thus 1/2. The operation can be repeated, and subsamples further dichotomically splitted (1/4, 1/8, etc.) until reaching the desired amount of organisms in the subsample (2000–5000). Only one subsample per sample is then imaged, with no replicate. The subsample is poured in a cylindrical transparent tank containing 5 L of filtered seawater (smallest mesh filter = 5 μm) and gently stirred to prevent the organisms from sinking at the bottom of the tank. Then, a peristaltic pump drives the filtered seawater and the organisms to the flowcell (10 × 10 mm inside cross section) mounted between the camera and the illumination system, where they are imaged at 16 fps, at a 1 L min^{-1} flowrate (note that a 2020 ZooCAM software update now enables a 30 fps image capture rate). The ZooCAM optical set-up features a 10 mm depth of

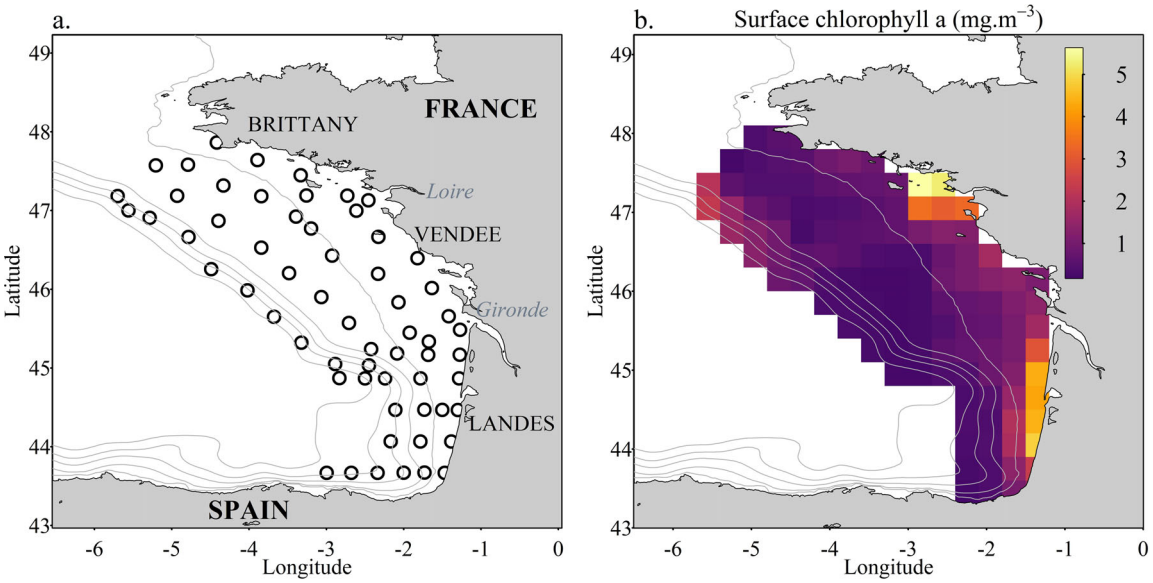

Fig. 1. (**a**) Location of the 61 zooplankton samples collected during the 2016 PELGAS survey. (**b**) Map of the surface chlorophyll-a total concentration (mg m^{-3}) in spring 2016. Light gray lines: 100, 200, 500, 1000, and 2000 m isobaths.

field, and a 13.6 × 10.9 mm field of view, encompassing the inner width of the flowcell. Objects touching the edges of the images at the inlet or the outlet of the flowcell (partially imaged objects) were taken into account in this study. For a detailed description of the ZooCAM imaging specification, the reader is invited to read Colas et al. (2018). For each sample, the whole subsample is imaged. For each subsample, the tank, the stirring device and the tubing were carefully rinsed with filtered seawater to ensure that all the organisms from the subsample were pumped and imaged. After being imaged, the zooplankton subsample was recovered on a 200 μm mesh size sieve and the whole sample was preserved in 4% formaldehyde (final concentration).

The ZooCAM software controls and synchronizes the pump, the stirring, the illumination system and the camera. Also, it provides all the necessary tools for the zooplankton samples imaging analysis: images acquisition, images process to create individual vignettes of each imaged object, and associated morphological features, semi-automatic identification with machine learning tools (training sets and various classifiers), and expert visual inspection of machine identified objects. Depending on the initial water content of the tank and the rinsing, a ZooCAM run can generate up to 10 k small size (~ 1 megabytes) raw images for each sample, from which the individual organism vignettes will be extracted. A ZooCAM run on a live sample often generates up to 5000–10,000 individual organisms vignettes.

Samples imaging with the ZooScan

The preserved samples were digitized with the ZooScan, a flatbed scanner creating 16-bit gray-level high-resolution images (2400 dpi, pixel size: 10.6 μm, Gorsky et al. 2010). The ZooScan creates a large, single image for each scan that contains several hundreds to 1500–2000 organisms depending on the size of the imaged organisms.

Before digitization, formaldehyde was removed and the sample rinsed with freshwater. The samples were then size-fractionated with a 1 mm sieve, into organisms larger and smaller than 1 mm size fractions, to limit the under-representation of large and rare objects due to subsampling. Then, a Motoda splitter was used to subsample each fraction separately to obtain subsamples containing between 500 and 1500 objects. Each subsample was imaged separately after manual separation of objects on the scanning tray, to limit the number of overlapping objects (Vandromme et al. 2012).

Image processing

For both instruments, image processing consists in the background subtraction with a blank and empty background image, a thresholding, for each raw image, followed by the segmentation of each object imaged. Each segmented object is then automatically processed individually for the extraction of its morphological features. Remaining touching objects spotted on the individual vignettes from the ZooScan were digitally manually separated with a ZooProcess tool to improve the quality of further identifications and counts. ZooCAM does not offer such a tool. Details about the images processing associated with the ZooScan and the ZooCAM can be found in Gorsky et al. (2010) and in Colas et al. (2018), respectively. ZooScan images were processed with the custom made, ImageJ based, ZooProcess (v7.39, 10 April 2020) software. The ZooProcess manual is available online (Jalabert et al. 2022). ZooCAM images were processed with the ZooCAM custom made software which uses the MIL (Matrox Imaging Library, Dorval, Québec, Canada) as the individual object processing kernel. The ZooCAM software was developed in Csharp language, and is not currently open source.

Taxonomic identification and selection of taxa

All individual vignettes from both instruments were classified with the online application Ecotaxa (Picheral et al. 2017). This online tool enables the automatic classification of all the individual vignettes into taxonomic categories. The classification was then visually inspected and manually validated or corrected when necessary. A total of 113,628 vignettes from the ZooScan and 184,335 vignettes from the ZooCAM, for objects larger than 0.3 mm ESD, were initially sorted into 35 zooplankton and non-zooplankton categories. Non-living and non-zooplankton categories (i.e., detritus, fibers, bubbles, artifacts, and phytoplankton) and overlapping objects were removed from those initial datasets (Table 1, gray lines). All remaining zooplankton individuals were used for an assessment of the instruments interoperable size range based on the computation of Normalized Biovolume-Size Spectra (NB-SS, see "Computation of zooplankton variables" and the "Assessment" sections below). This analysis led to the removal of a few dozens of very large objects from the initial datasets, resulting in working datasets composed of 113,390 and 184,202 individuals, for ZooScan and ZooCAM, respectively. Then, poorly represented taxa for which occurrences at stations combining the two instrument datasets were smaller than 30 (maximum occurrences is 122, i.e., twice 61 stations), as well as non-taxonomically resolved objects (identified as "Other") were not taken into account in the zooplankton variables computation and in community structure analyses. Finally, the zooplankton communities as seen by the two instruments were compared using 27 taxonomic groups (Table 1, Fig. 2). Some taxonomic groups aggregate a diversity of organisms. "Hydrozoa" include gelatinous medusa-like organisms, except the siphonophores, which were sufficiently well identified to constitute a separate group. "Thecosomata" integrate Limacinidae and Pteropods. "Shrimp-like" gather all adult crustaceans such as Euphausiids, Amphipods, and Decapods, copepods excluded. "Harosa" gather the protozoa such as large Foraminifera, and Acantharia. Finally, "Actinopterygii" stands for fish larvae (Table 1, Fig. 2). Unidentified planktonic objects represented 5.9% and 1.7% of ZooCAM abundances and biovolumes, and 0.8% and 0.5% of ZooScan abundances and biovolumes.

Table 1. Taxonomic list of the 35 initially identified taxa and objects groups, and the 27 selected groups' subset, and their abundances (ind m^{-3}), biovolumes (mm^3 m^{-3}), and associated proportions in the communities (%) for each instrument.

Taxa	ZooCAM				ZooScan				# occurrences
Units	Ind m^{-3}	%	mm^3 m^{-3}	%	Ind m^{-3}	%	mm^3 m^{-3}	%	#/122
1-Actinopterygii	1.51	0.01 (*0.03*)	1.84	0.11 (*0.21*)	1.85	0.03 (*0.04*)	1.51	0.14 (*0.21*)	48
2-Actinopterygii egg	20.14	0.16 (*0.38*)	21.03	1.24 (*2.37*)	7.55	0.1 (*0.16*)	4.82	0.46 (*0.66*)	72
3-Annelida larvae	3.01	0.02 (*0.06*)	0.2	0.01 (*0.02*)	10.25	0.14 (*0.21*)	0.56	0.05 (*0.08*)	41
4-Annelida	5.8	0.05 (*0.11*)	4.3	0.25 (*0.48*)	6.76	0.09 (*0.14*)	2.18	0.21 (*0.3*)	66
5-Bivalvia	24.08	0.19 (*0.45*)	0.41	0.02 (*0.05*)	45.57	0.62 (*0.94*)	0.89	0.09 (*0.12*)	75
6-Calanoida	1677.76	13.07 (*31.48*)	193.59	11.42 (*21.77*)	1472.46	19.99 (*30.45*)	159.09	15.19 (*21.65*)	122
7-Acartiidae	620.7	4.83 (*11.65*)	94.81	5.59 (*10.66*)	779.28	10.58 (*16.12*)	101.15	9.66 (*13.76*)	121
8-Calanidae	100.27	0.78 (*1.88*)	164.21	9.68 (*18.47*)	105.66	1.43 (*2.19*)	160.43	15.32 (*21.83*)	121
9-Centropagidae	66.73	0.52 (*1.25*)	28.58	1.69 (*3.21*)	105.83	1.44 (*2.19*)	33.23	3.17 (*4.52*)	118
10-Euchaetidae	16.4	0.13 (*0.31*)	18.96	1.12 (*2.13*)	35.48	0.48 (*0.73*)	27.71	2.65 (*3.77*)	101
11-Metridinidae	12.44	0.1 (*0.23*)	15.9	0.94 (*1.79*)	36.89	0.5 (*0.76*)	33.21	3.17 (*4.52*)	96
12-Temoridae	310.62	2.42 (*5.83*)	58.65	3.46 (*6.6*)	320.76	4.35 (*6.63*)	54.32	5.19 (*7.39*)	114
13-Cyclopoida	899.58	7.01 (*16.88*)	39.17	2.31 (*4.41*)	817.28	11.1 (*16.9*)	31.08	2.97 (*4.23*)	122
14-Harpacticoida	77.45	0.6 (*1.45*)	3.58	0.21 (*0.4*)	86.2	1.17 (*1.78*)	3.83	0.37 (*0.52*)	103
15-Poecilostomatoida	324.18	2.52 (*6.08*)	10.26	0.61 (*1.15*)	240.67	3.27 (*4.98*)	8.74	0.83 (*1.19*)	122
16-Cirripedia larvae	140.37	1.09 (*2.63*)	4.93	0.29 (*0.55*)	144.93	1.97 (*3*)	4.56	0.44 (*0.62*)	101
17-Cladocera	199.44	1.55 (*3.74*)	14.52	0.86 (*1.63*)	216.44	2.94 (*4.48*)	13.01	1.24 (*1.77*)	88
18-crustacea nauplii	59.8	0.47 (*1.12*)	2.51	0.15 (*0.28*)	38.72	0.53 (*0.8*)	1.32	0.13 (*0.18*)	118
19-shrimp like	17.19	0.13 (*0.32*)	28.71	1.69 (*3.23*)	20.88	0.28 (*0.43*)	33.21	3.17 (*4.52*)	115
20-shrimp like larvae	8.91	0.07 (*0.17*)	2.32	0.14 (*0.26*)	7.7	0.1 (*0.16*)	1.86	0.18 (*0.25*)	73
21-Echinodermata	41.47	0.32 (*0.78*)	6.99	0.41 (*0.79*)	25.67	0.35 (*0.53*)	3.39	0.32 (*0.46*)	76
22-Harosa	304.85	2.37 (*5.72*)	34.16	2.01 (*3.84*)	5.09	0.07 (*0.11*)	0.13	0.01 (*0.02*)	70
23-Appendicularia	191.85	1.49 (*3.6*)	29.74	1.75 (*3.35*)	179.88	2.44 (*3.72*)	15.8	1.51 (*2.15*)	112
24-Chaetognatha	24.2	0.19 (*0.45*)	20.59	1.21 (*2.32*)	18.56	0.25 (*0.38*)	17.49	1.67 (*2.38*)	94
25-hydrozoa	27.62	0.22 (*0.52*)	19.49	1.15 (*2.19*)	39.08	0.53 (*0.81*)	10.63	1.01 (*1.45*)	97
26-Siphonophorae	83.13	0.65 (*1.56*)	66.49	3.92 (*7.48*)	6.47	0.09 (*0.13*)	8.37	0.8 (*1.14*)	104
27-Thecosomata	70.12	0.55 (*1.32*)	3.16	0.19 (*0.36*)	59.59	0.81 (*1.23*)	2.35	0.22 (*0.32*)	97
Total (%)		41.51 (*100*)		52.43 (*100*)		65.65 (*100*)		70.17 (*100*)	
Non-living	6149.13	47.89	684.45	40.37	2155.91	29.27	254.31	24.28	122
Multiples	58.67	0.46	41.6	2.45	56.22	0.76	40.56	3.87	121
Phytoplankton	892.51	6.95	62.08	3.66	257.02	3.49	12.3	1.17	107
Other	395.36	3.08	16.85	0.99	43.83	0.6	3.57	0.34	121
Bryozoa cyphonaute	12.14	0.09	0.32	0.02	13.51	0.18	0.33	0.03	30
Ctenophora	3.02	0.02	0.64	0.04	2.24	0.03	0.18	0.02	25
Egg sac	0.78	0.01	0.33	0.02	1.45	0.02	0.76	0.07	28
Thaliacea	0.01	< 0.01	0.11	0.01	0.07	< 0.01	0.48	0.05	4
Total (%)		58.5		47.56		34.35		29.83	

Italic numbers in the proportion columns represent the proportion of each selected taxa, for each variable, in the subset of selected taxa, for each instrument. "Occurrence" is the number of times a taxa or group is present at a station, combining the two instruments datasets (maximum occurrences is 122, i.e., twice 61 stations). The taxa highlighted in gray were not used for the community analyses, either because being non-living, imaging artifacts (e.g., multiples), not zooplanktonic (e.g., phytoplankton), unidentifiable (e.g. "other"), or too poorly represented in the datasets (Occurrence ≤30).

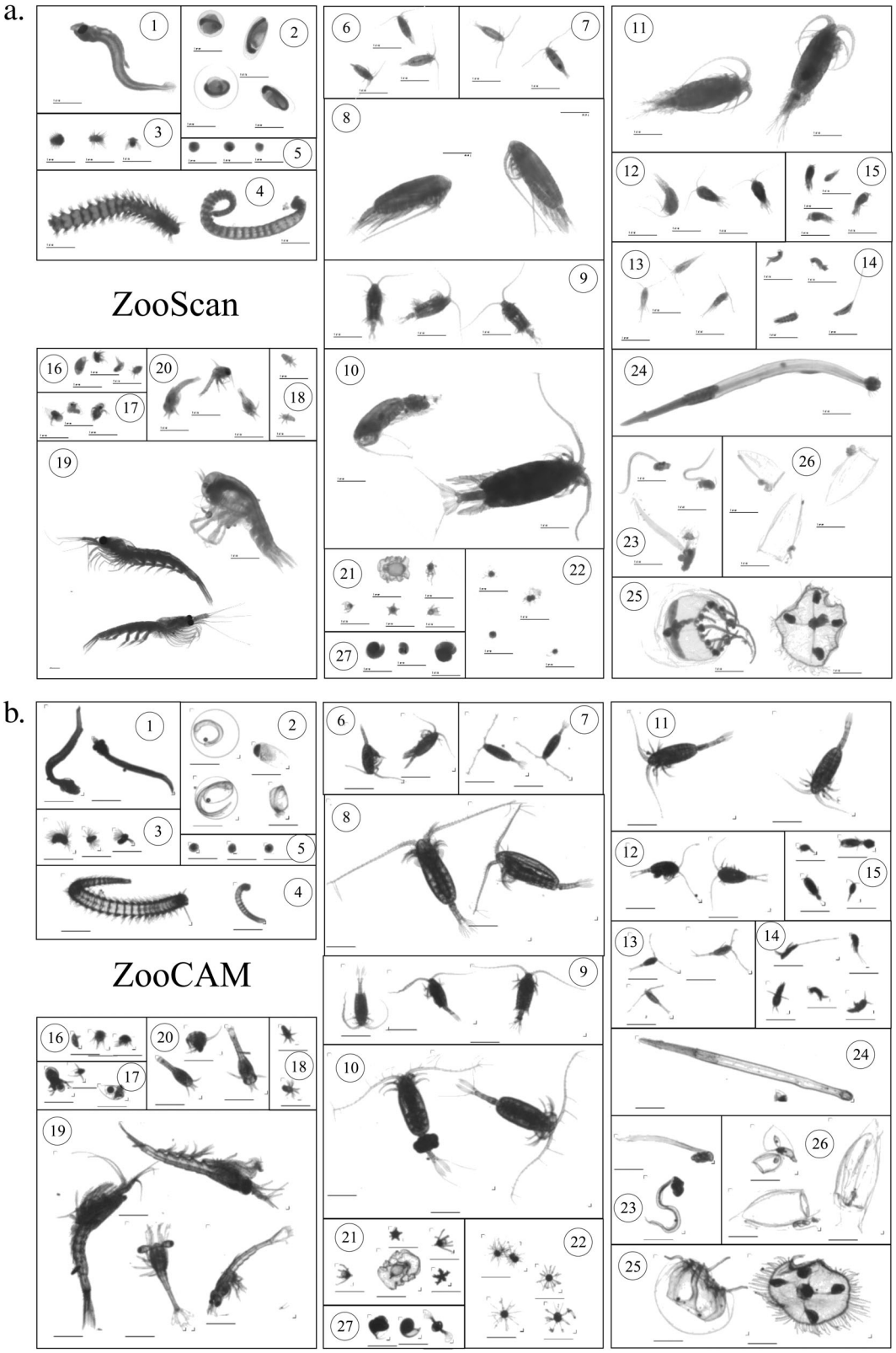

Fig. 2. (**a**) Top panel: Images of organisms belonging to the taxa used for the community analyses as seen by the ZooScan. (**b**) Bottom panel: Images of organisms belonging to the taxa used for the community analyses as seen by the ZooCAM. The legends of the numbers associated to each taxa can be found in Table 1 (first column). Note that all organisms shown in this figure are scaled, except the two shrimp like individuals (19) in the ZooScan (**a**) panel, that were reduced in size (scale 1/2) to fit in the box. The black line in every image is 1 mm long.

Computation of zooplankton variables

The computation of zooplankton working variables and following data analyses were performed using the R statistical language version 4.0.3 (R Core Team, 2020) and the Matlab R2021b software with the machine learning and statistics toolbox.

Total counts and mean sizes computation

For both instruments, the subsampling ratios were accounted for calculating total abundances (counts expressed in number of individuals) by stations and by taxonomic groups.

Individual sizes were computed as Equivalent Spherical Diameter (ESD, expressed in mm) as follow:

$$\mathrm{ESD} = 2 \times \sqrt{\left(\frac{\mathrm{Area}}{\pi}\right)}$$

where Area is the objects' surface converted from pixels to mm^2.

Mean sizes (expressed in mm) were computed by stations and by taxonomic groups.

Normalized Biovolume-Size Spectra computation

Individual spherical biovolumes (SBv, expressed in mm^3) were calculated with the following equation:

$$\mathrm{SBv} = \frac{4}{3} \times \pi \times \left(\frac{\mathrm{ESD}}{2}\right)^3$$

where ESD is the objects' individual size expressed in mm.

Individual SBv were used to construct NB-SS (Platt and Denman 1978) at each sampling station. The NB-SS is a zooplankton community size structure descriptor traditionally used to estimate the biomass and energy transfer across size classes (Zhou 2006). The NB-SS computation was initially based on the [0.01–100] mm^3 size range. The size classes were defined by intervals noted $[\log(x_n); \log(x_{n+1})]$ of length $\log(x_{n+1}) - \log(x_n) = \log(k)$ being constant with $k = 2$. Each size class n was represented on the x-axis by its nominal value (mm^3) calculated as $(\log(x_n) + \log(x_{n+1}))/2$. The choice of $k = 2$ implies that size classes are doubling in width at each iteration. Therefore, the resulting size classes' vector used to construct the NB-SS was composed of 14 size classes, and encompass the entire size range of the imaged organisms. The y-axis represents the normalized biovolume (m^{-3}) on a log scale, calculated as the sum of individual biovolumes within the size classes (mm^3), multiplied by the subsampling ratio (unitless) and divided by the sampled water volume (m^3), and normalized by the width of the size class (mm^{-3}). Then, a linear regression was fitted to the NB-SS data from the mode of the NB-SS (i.e., the size class in which the NB-SS shows its maximum value) to the last size class. The slope of the linear regression informs on the proportion of small individuals compared to the large ones, with a flatter slope interpreted as an increase of biovolume in the large size classes, hence a greater proportion of large organisms in the sample (Zhou 2006).

Assessment

Determination of the instruments interoperable size range

Prior to any numerical analysis, the NB-SS were used to define the size interval in which to compare the two instruments. An iterative procedure was set up: (1) the mean NB-SS for each instrument were computed across the entire size range, i.e., [0.01–100] mm^3 corresponding to [0.3–14.24] mm ESD and $n_0 = 14$ size bins, (2) the slopes of those mean NB-SS were calculated, and compared using an Analysis of covariance (ANCOVA), and (3) if the slopes were statistically significantly different, the operation was repeated removing the last size bin (first iteration, $n_1 = 13$ size bins, second iteration, $n_2 = 12$ bins, etc.). In the initial case (n_0, 14 size classes and [0.3–14.24] mm ESD size range), the two mean NB-SS and their slopes were different (ZooScan mean NB-SS slope $= -1.22 \pm 0.06$; ZooCAM mean NB-SS slope $= -0.99 \pm 0.08$). The discrepancy between

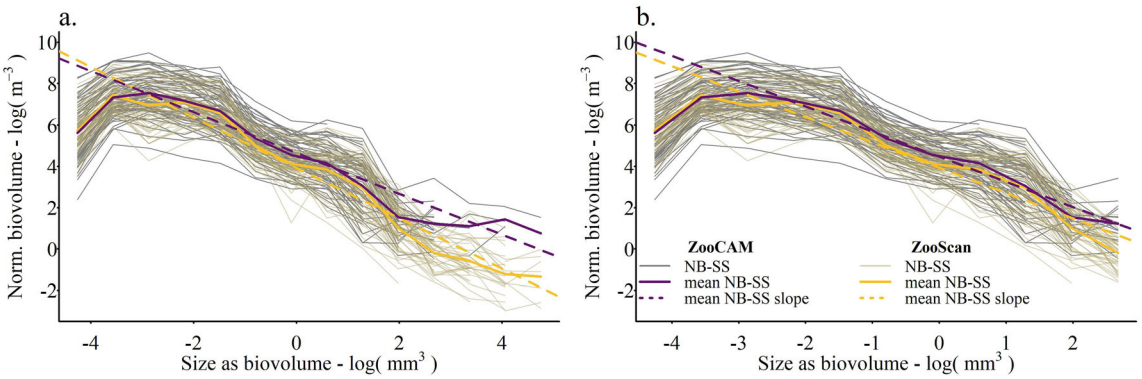

Fig. 3. (**a**) Normalized Biovolume–Size Spectra (NB-SS) computed in the [0.01–100] mm^3 biovolume range corresponding to the [0.3–14.24] mm ESD size range, ($n = 14$ size bins) and (**b**) in the [0.01–20.48] mm^3 biovolume range corresponding to the [0.3–3.39] mm ESD size range ($n = 11$ size bins) on which mean NB-SS slopes are equal. Thin lines: ZooScan (beige) and ZooCAM (gray) NB-SS computed at each sampling station ($n = 61$). Bold yellow curves: ZooScan mean NB-SS. Bold purple curves: ZooCAM mean NB-SS. Dashed lines: mean NB-SS slopes.

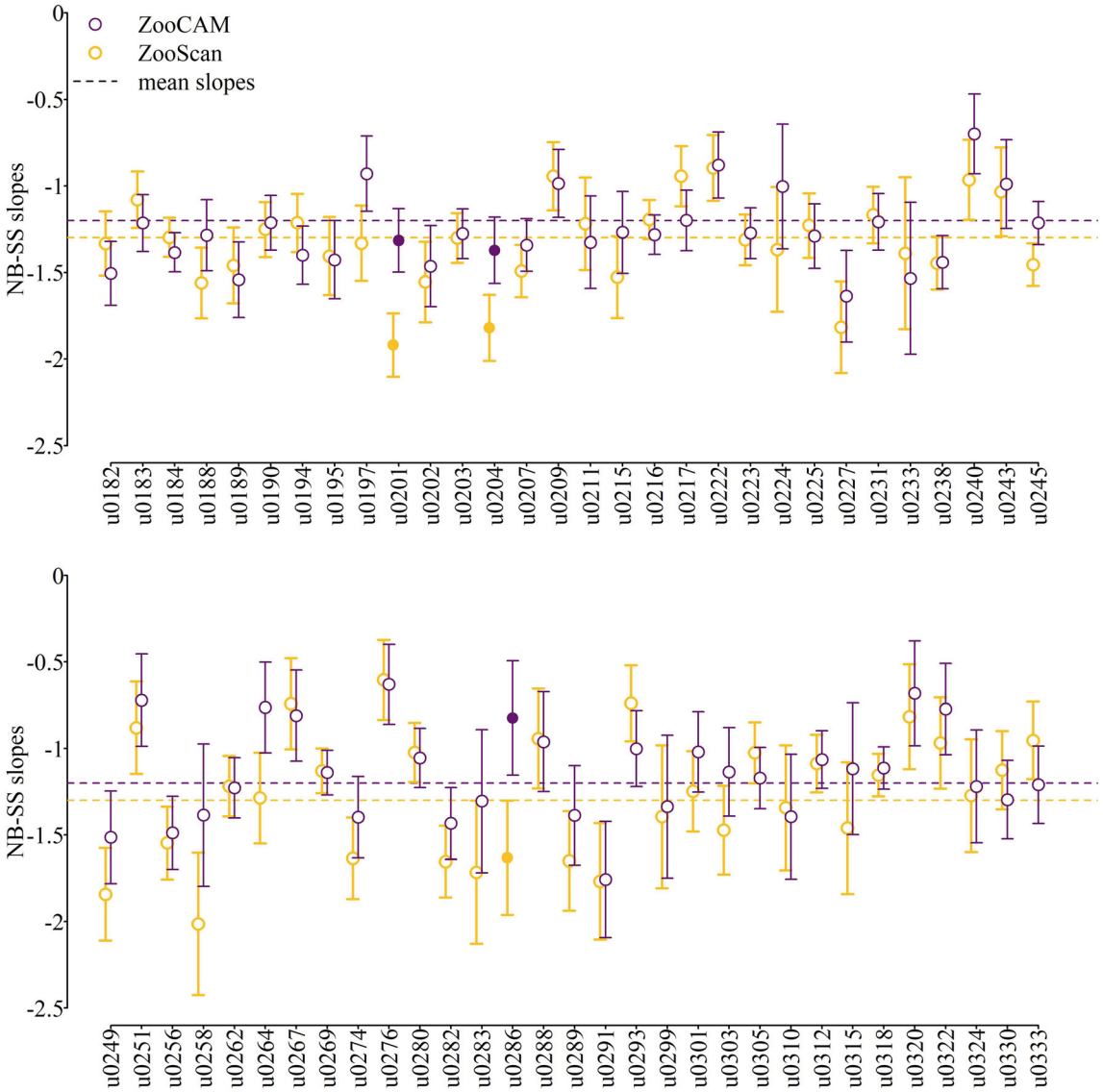

Fig. 4. NB-SS slopes and their confidence intervals calculated for the 61 sampling stations (yellow, ZooScan; purple, ZooCAM). Open symbols: stations for which there is no significant differences between ZooScan and ZooCAM NB-SS slopes. Closed symbols: stations for which there is a significant difference between ZooScan and ZooCAM NB-SS slopes. Dashed lines: mean NB-SS slopes. The stations' names are on the x-axis. The slopes were calculated in the [0.3–3.39] mm ESD size range.

the two mean NB-SS was observed in the largest size classes where larger normalized biovolumes were estimated with the ZooCAM data (Fig. 3a). On the contrary, the mean NB-SS were similar in the small size classes. The procedure was repeated four times and the slopes of the two mean NB-SS eventually became not statistically different with an 11 size classes' vector. The ZooScan mean NB-SS slopes was equal to -1.23 ± 0.1, and that of the ZooCAM was equal to -1.22 ± 0.06, in the [0.01–20.48] mm^3 biovolume range corresponding to the [0.3–3.39] mm ESD size range (Fig. 3b). This size range will be referred to as large mesozooplankton size range hereafter, as the mesozooplankton is traditionally defined as organisms in the [0.2–2] mm size range (Sieburth et al. 1978), and is from now on our working size range. ANCOVA tests were performed using Matlab and the specific functions aoctool and multcompare.

Comparisons of NB-SS slopes by stations

The ZooScan and the ZooCAM were first compared with the NB-SS slopes calculated at each sampling station using an ANCOVA test. NB-SS slopes showed a good agreement between both instruments (Fig. 4). Three stations had significantly different slopes (u0201, u0204, and u0286, Fig. 4). All three had flatter slopes with the ZooCAM data, indicating that the ZooCAM detected more large objects than the ZooScan at these stations. A linear regression fitted to the

Table 2. Linear regression parameters and Spearman correlation coefficient and *p*-value for the variables calculated by sampling stations.

Variables by station	*n*	Linear regression equation	R^2	*p*-value	Cor. Coefficient	p-value
NB-SS slopes	58	$y = 0.88x - 0.2$	0.56	7.37×10^{-12}	–	–
Mean ESD	60	$y = 1.13x - 0.06$	0.87	$<2 \times 10^{-16}$	0.94	$<2 \times 10^{-16}$
Total counts	58	$y = 0.67x + 0.08$	0.53	9.37×10^{-11}	0.73	9.37×10^{-11}

slopes by stations between the ZooScan and ZooCAM data without taking into account those with a significant difference ($n = 58$) had an estimated slope of 0.88 (p-value <0.05, $R^2 = 0.56$) indicating a small difference between datasets (Table 2). The spatial patterns over the Bay of Biscay continental shelf were similar for the two instruments (Supporting Information Fig. S1).

Mean sizes and abundances by stations

Then, the two instruments mean individuals sizes and total counts calculated by station were compared. Linear regressions were performed on mean sizes and log-transformed total counts between the ZooScan and the ZooCAM data. Spearman correlation tests were run to estimate the correlations between the values obtained with both instruments. For each variable, a procedure to find the stations where the ZooScan and the ZooCAM values were abnormally different was applied before performing the regressions and the correlation tests. The data points for which such an abnormal difference was detected were not included in the analyses, albeit being shown in the figures. The procedure is described in details in the Supporting Information section "Abnormal differences between instruments test procedure."

The mean sizes (ESD) calculated at each sampling station ranged from 0.49 to 0.76 mm (mean = 0.57 ± 0.06 mm) in the ZooScan data, and from 0.51 to 0.73 mm (mean = 0.58 ± 0.05 mm) in the ZooCAM data. Mean size values by station were consistent between instruments and only one station had a ZooCAM mean size much larger than the ZooScan's (Sta. U0286, closed symbol in Fig. 5a, and in Supporting Information Fig. S4a,b, excluded from the linear regression and the correlation test). The linear regression was fitted to the 60 remaining data points and the two datasets were significantly correlated ($r = 0.94$, Table 2), and depicted similar spatial patterns (Supporting Information Fig. S4).

The total abundances by stations ranged from 919 individuals m^{-3} to 14,140 individuals m^{-3} (mean = 4,840 ± 3,550 ind m^{-3}) in the ZooScan data and from 361 individuals m^{-3} to 19,525 individuals m^{-3} (mean = 5,330 ± 4,245 ind m^{-3}) in the ZooCAM data. Three stations showed abnormally different total counts between instruments. One station (U0203) showed higher ZooCAM total counts, while

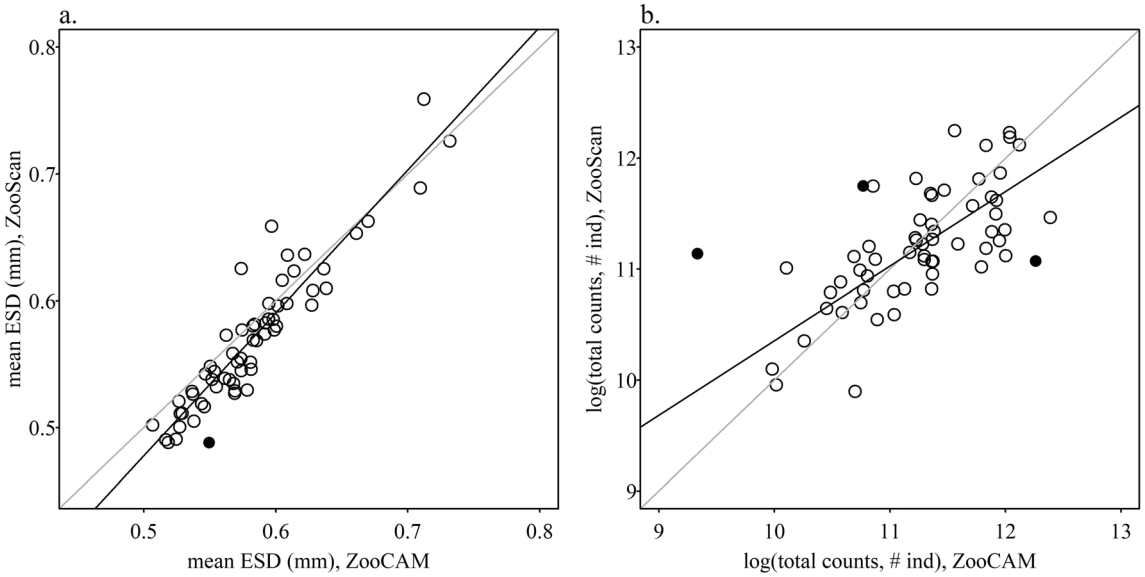

Fig. 5. Linear regressions between ZooCAM (x-axis) and ZooScan (y-axis) stations data performed on (**a**) mean ESD (mm; $n = 60$, open symbols) and (**b**) total counts (number [#] of individuals; $n = 58$, open symbols). The gray line represent the 1 : 1 line. Stations with abnormally large differences between the ZooScan and the ZooCAM values were not included in the regressions (closed symbols).

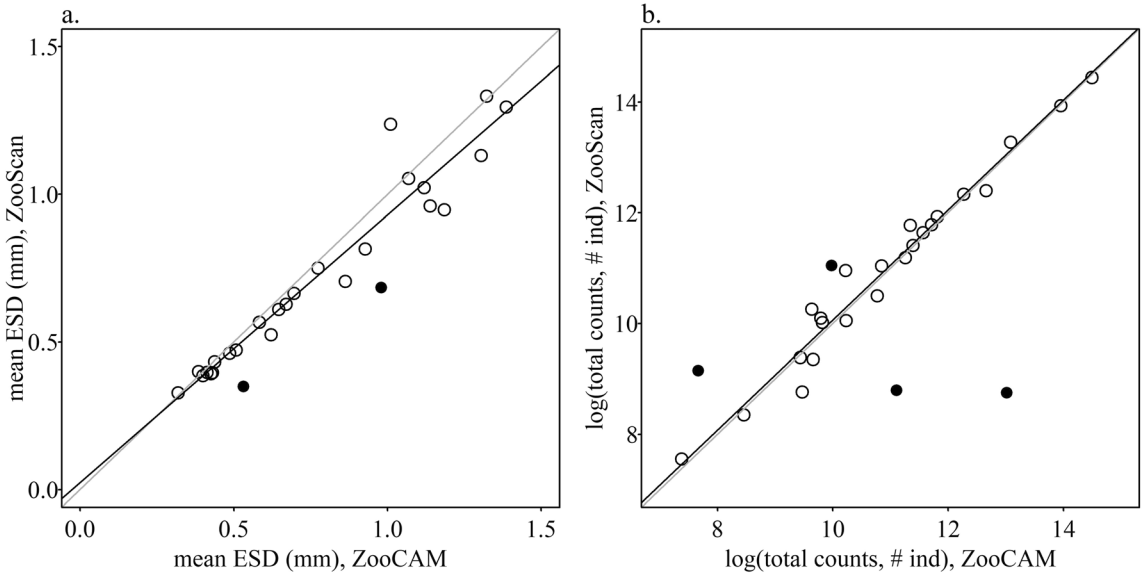

Fig. 6. Linear regressions between ZooCAM (x-axis) and ZooScan (y-axis) taxa data performed on (**a**) mean ESD (mm; $n = 25$, open symbols) and (**b**) total counts (number [#] of individuals; $n = 23$, open symbols). The gray line represent is the 1 : 1 line. Taxa with abnormally large differences between the ZooScan and the ZooCAM values were not included in the regressions (closed symbols).

the two other stations (U0315 and U0320) showed higher ZooScan total counts (Fig. 5b). These stations were excluded from the linear regression and the correlation test. The linear regression was fitted to 58 remaining data points and revealed a robust agreement and a significant correlation between the two datasets (Table 2), and depicted similar spatial patterns (Supporting Information Fig. S5).

Comparison of the community composition

The abundances proportions (in %) of each taxa ($n = 27$) were compared over the whole Bay of Biscay continental shelf, between the two instruments. Only the taxa contributing at least 1% to the total abundance were considered (Table 1). The Calanoida represented the largest part of the total abundance for both instruments followed by the Cyclopoida and the Acartiidae. On the contrary, the Harosa and to a lesser extend the Siphonophorae and the Crustacea nauplii represented more than 1% of the total abundance estimated with the ZooCAM but < 1% within the ZooScan data. Pairwise Wilcoxon tests run on the taxa abundances proportions calculated at each station showed no significant differences at any stations, indicating that the community composition was highly similar between both instruments.

The ZooScan and ZooCAM total counts and mean sizes calculated by taxa were also compared. The procedure to detect abnormally large differences between ZooCAM and ZooScan taxa data was applied. The procedure is described in details in the Supporting Information section "Abnormal differences between instruments test procedure."

The mean ESD by taxa were very similar between instruments (Fig. 6a). The Harosa and the Hydrozoans were the two taxa identified showing abnormally large differences between ZooCAM and ZooScan data. They both displayed smaller sizes with the ZooScan data, and were excluded from the linear regression and the correlation test. A linear regression was fitted to the 25 remaining taxa data points and revealed a robust agreement and a significant correlation between the two mean sizes datasets (Table 3). The total counts by taxa were also consistent for both instruments but showed four taxa for which differences between instruments were abnormally large (Fig. 6b). The Annelida larvae and the Metridinidae showed higher total counts with the ZooScan, whereas the Harosa and the Siphonophorae showed higher total counts with the ZooCAM. These taxa were excluded from the linear regression and the correlation test. A linear regression was fitted to the 23 remaining taxa data points and revealed a robust agreement and a

Table 3. Linear regression parameters and Spearman correlation coefficient and *p*-value for the variables calculated by taxa.

Variables by taxa	*n*	Linear regression equation	R^2	*p*-value	Cor. coefficient	*p*-value
Mean ESD	25	$y = 0.91x + 0.05$	0.93	4.78×10^{-15}	0.97	4.78×10^{-15}
Total counts	23	$y = 0.99x + 0.04$	0.97	$<2 \times 10^{-16}$	0.98	$<2 \times 10^{-16}$

significant correlation between the two total counts datasets (Table 3).

Comparison of the community spatial structure

To assess the differences between the zooplankton community spatial patterns depicted by the ZooScan and the ZooCAM, the taxa abundances (individuals m^{-3}) calculated by stations were spatially smoothed through a block averaging procedure (Petitgas et al. 2009, 2014) and gridded over a common spatial grid. The grid mesh size was set at 0.3° in both latitude and longitude. The grid origin x0 was initially positioned at 43° N and 6° W and then drawn randomly within a two cells radius, 300 times. Data were averaged in each grid cell for every origin position, in order to minimize the influence of the origin position on gridded values. Finally, 300 mean values were averaged to calculate a spatially smoothed estimate in each grid cell. The block averaging procedure was realized with the EchoR R library (Doray et al. 2013).

The gridded abundances data were log-transformed to reduce the skewness in their distributions. Two separated Principal Component Analyses (PCA, one analysis for each instrument) were used to summarize the data into principal components

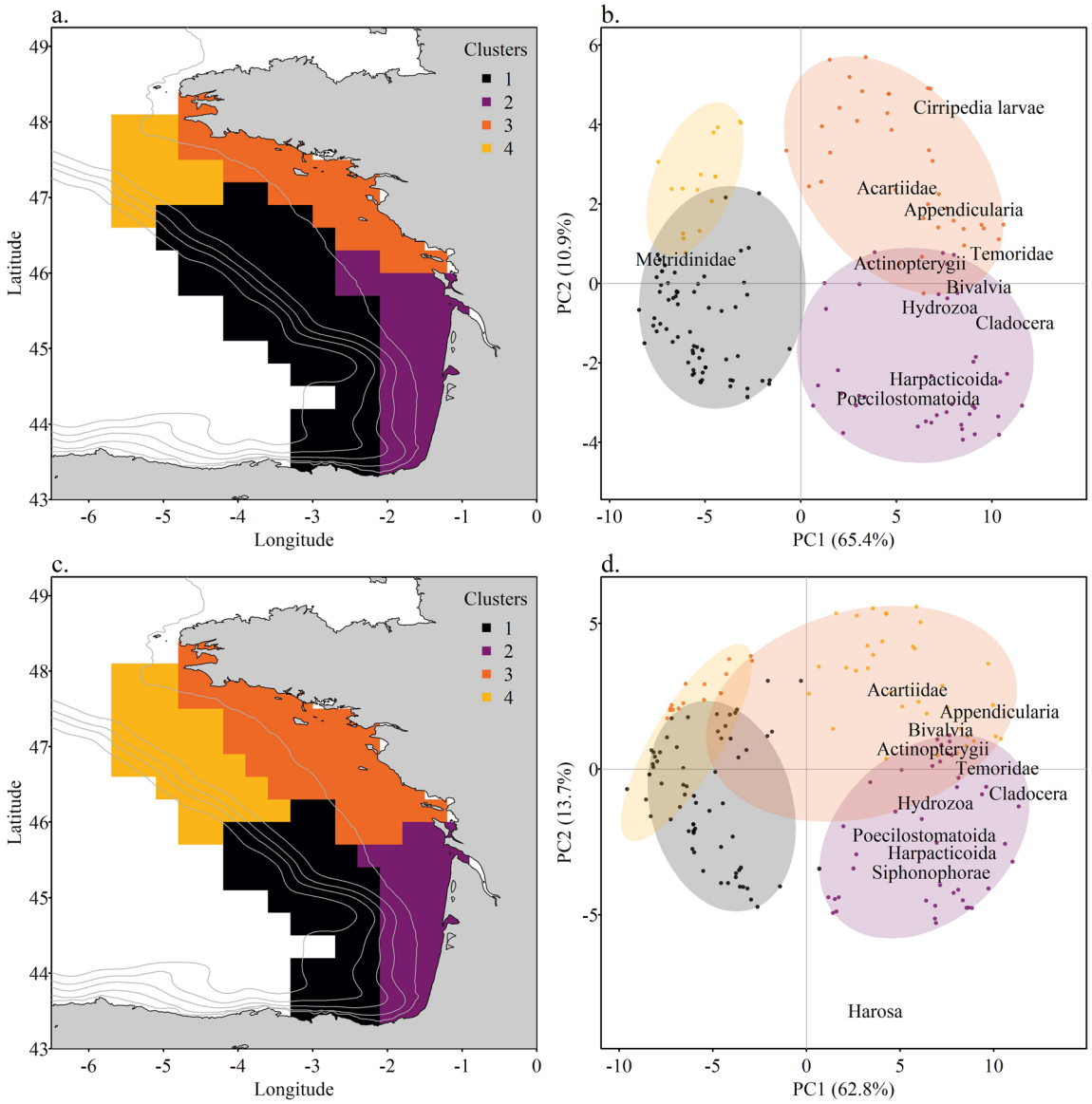

Fig. 7. (**a–c**) Zooplankton community spatial structure derived from the hierarchical clustering of grid cells' coordinates in the abundances PCA factorial space (four first principal components), based on (**a**) the ZooScan data and (**c**) the ZooCAM data. (**b–d**) Biplots of the two first principal components of the abundances PCA based on (**b**) the ZooScan data and (**d**) the ZooCAM data. The ellipses and dots colors correspond to the cluster colors on the maps. Only the taxa having a correlation coefficient higher than 0.8 with the two first principal components are shown.

accounting for the largest part of the data variability. Then, the spatial structure of the zooplankton community was identified with a spatially constrained Hierarchical Agglomerative Clustering applied on the grid cells' coordinates in each PCA factorial space (Ward's method with euclidean distance matrix). The function hclustgeo in R language was used. Grid cell clusters were mapped to characterize the spatial structure of the zooplankton community. A biplot was also constructed with the grid cells' and the taxonomic groups' coordinates on the two first principal components to identify which taxa correlate to the spatial patterns.

For both instruments, the hierarchical clustering was done on the four first principal components of the abundance PCA, explaining 85% of the abundances datasets total variance. The abundances' spatial patterns were composed of four clusters and are presented with the most characteristic taxa of these spatial structures in Fig. 7. The zooplankton community spatial patterns were highly similar between the ZooScan and the ZooCAM and highlighted a coastal—offshore and a North–South gradients (Fig. 7a,c). Only few differences were noted in the clusters' limits. The northern coastal cluster (cluster 3), which gathered grid cells along the Brittany and the Vendee coast extended further on the continental shelf with the ZooCAM data. The spatial limit between the southern and northern offshore clusters (clusters 1 and cluster 4, respectively) was located at 46°N with the ZooCAM data and further north, at 47°N, with the ZooScan data (Fig. 7a,c). For both instruments, the Appendicularia, the fish larvae ("Actinopterygii"), the Cladocera, the Bivalvia, the Hydrozoan and the small copepods Acartiidae, Temoridae, Harpacticoida, and Poecilostomatoida were characteristic of coastal areas (Fig. 7b,d). Differences were noted for the Siphonophorae and the Harosa which indicated the southern coastal cluster of the ZooCAM data (Fig. 7d) but not that of the ZooScan data. On the contrary, the Cirripedia larvae indicated the northern coastal cluster while the large copepods Metridinidae marked the offshore clusters only for the ZooScan data (Fig. 7b).

Discussion

The objective of this study was to compare the use of two imaging systems, the ZooScan (flatbed scanner) and the ZooCAM (in-flow imaging) to depict the taxonomic composition, the size structure and the spatial patterns of the zooplankton community in the Bay of Biscay in spring 2016. The good agreement between these two instruments was demonstrated on the large mesozooplankton size range, i.e., [0.3–3.39] mm ESD. This specific size range extends further than the traditional size range defining mesozooplankton organisms within the range [0.2–2] mm ESD (Sieburth et al. 1978). In a preliminary study, Colas et al. (2018) described the good agreement between the ZooScan and the ZooCAM in the Iroise Sea with nine samples and 10 taxa only, without exploring the zooplankton spatial patterns. Our study strengthen and improve these preliminary results showing the agreement between the two instruments in terms of abundances, mean sizes, size structure, biovolumes (Supporting Information), community composition, and community spatial patterns, using 61 samples and 27 taxa, over a much larger area encompassing most of the hydrographic, bathymetric and production conditions that can be encountered in temperate regions. Community differences across stations between the two instruments resulted in similar spatial patterns identified through spatially resolved taxa abundances and biovolumes. For both instruments, spatial gradients were mainly driven by the prevailing importance of small copepods, meroplanktonic and gelatinous organisms in coastal areas opposed to large copepods offshore. We therefore consider that our initial working hypothesis is validated: the ZooScan and the ZooCAM are interoperable.

Yet, differences between the two instruments have been identified in both stations and taxa datasets. The two systems were used following different data collection strategies: the ZooCAM was used on-board on live organisms while the ZooScan was used in the lab on the same but preserved samples. Also, each instruments did not image the exact same aliquot of the sample. Therefore, the discrepancies found in the results are discussed hereafter according to three main points: the differences in the sample preparation before the image acquisition, the differences in the imaging technique and the differences in the image quality.

How can we explain the observed differences?

Sample preparation: Size fractionation and subsampling

The first difference between the two imaging instruments lies in their conceptual set up: the ZooScan is a steady flatbed scanner, and one cannot place too many objects at once on the surface of the scanner without increasing the number of touching objects (Vandromme et al. 2012). Touching objects should be avoided as much as possible to ensure good particle statistics. The ZooCAM is an in-flow instrument with fewer quantitative constraints. This difference lead to different sample preparation before the image acquisition. With the ZooScan, the samples are split into two size fractions (larger and smaller than 1 mm), that are subsampled separately with a Motoda splitter to obtain adequate numbers of objects to minimize their overlap on the scanning tray in each size fraction (see section Materials and procedures). The large objects are less abundant than the small ones, therefore the large objects size fraction subsampling ratio is usually comprised between 1 (no subsampling) and 1/8. Note here that to calculate quantitatively a sample's abundance after subsampling, one needs to multiply the number of objects counted in the subsample by the numerator of the subsampling ratio. As a consequence the abundances of large organisms imaged with the ZooScan are calculated using small subsampling ratios. On the contrary, the samples imaged with the ZooCAM are not size-fractioned before being

subsampled. Non-size-fractioned samples often require higher subsampling ratios (e.g., from 1/32 to 1/256) to obtain adequate numbers of objects in the aliquot to be imaged. In such a case, the large organisms may be under-sampled but their counts would be multiplied by a high subsampling ratio, possibly ending up with larger estimates than if they were subsampled apart from the small ones. These differences in the sample preparation protocols may have resulted in occasional higher estimates of large organisms in the ZooCAM dataset and contributed to the discrepancies in the largest size classes of the size spectra, flatter NB-SS slopes, and higher mean sizes as well as higher biovolumes, detected at few sampling stations in the ZooCAM dataset. The same reason could explain why ZooScan abundances and biovolumes for Sta. U0315 were three times higher than those of the ZooCAM. Besides differences in the number of objects imaged (2,443 for ZooCAM and 1,645 for ZooScan), the subsampling ratio of the small size fraction aliquot digitized with the ZooScan was four times higher than that of the aliquot imaged with the ZooCAM (1/128 vs 1/32).

Imaging on live vs preserved samples

Another cause of differences in the use of ZooCAM and ZooScan relates to whether the samples were live or fixed. The samples are imaged live on-board with the ZooCAM. On the contrary, samples are imaged after being preserved during several weeks, months, or years with the ZooScan. The classic formaldehyde-seawater preservation solution is known to affect the integrity of fragile zooplankton taxa and therefore may bias their size measurements and abundance estimates. For example, gelatinous zooplanktonic organisms are susceptible to formaldehyde-induced shrinkage and distortion (Nishikawa and Terazaki 1996; Beaulieu et al. 1999) and copepods and chaetognaths experience a significant loss of organic matter within such fixative solution (Omori 1978). The fixative effect therefore can be the cause of the observed difference of the mean size measures of Hydrozoans in our data. In addition, the mineralized protists, such as the acantharians (belonging to the overarching clade Harosa, along with radiolarians and foraminifera), are also degraded through the dissolution of their mineral skeleton if the fixative solution is not oversaturated with their skeleton main mineral (Beers and Stewart 1970). These protists that can be large and contribute significantly to the biomass of oceanic zooplankton are now considered completely underestimated in preserved seawater samples, as a result of damage by net collection and dissolution in the preservatives (Biard et al. 2016). The dissolution of mineralized protists, here gathered under the Harosa taxa, may explain their quasi absence in the ZooScan dataset (samples were preserved in buffered formaldehyde for 4 yr before digitization) compared to the much higher abundances, biovolumes and mean sizes estimates obtained when imaged live on-board with the ZooCAM, just after collection (fixative effect).

Imaging techniques

With the ZooScan, the images are acquired along a 2D plane where the objects are set horizontally, which is the best orientation to capture the objects' size and the silhouette. On the contrary, the ZooCAM is an in-flow imaging system in which the position of the object cannot be controlled when the images are captured. The zooplankton orientation in space may have two main effects: (1) make the identification more complicated for the algorithm and the experts when specific features are not visible, and (2) underestimate the size of objects if their longest axis is not captured (Colas et al. 2018). In our study, the Acartiidae, Metridinidae, and Euchaetidae contributed more to the total abundances and biovolumes in the ZooScan dataset than in the ZooCAM dataset. This result was essentially due to the difficulty to spot specific features in these taxa and differentiate them from non-identified calanoids (here gathered under the Calanoida taxa). The random orientation of copepods in the ZooCAM flow cell may have contributed to the observed slight underestimation of those copepods' abundances and biovolumes in the ZooCAM dataset in comparison to the ZooScan dataset (orientation effect), but have presumably not affected their size measurements, as ZooCAM and ZooScan data agree for those taxa. We conclude that the orientation effect may slightly bias the size measurements, yet non-significantly. This effect seem to be the cause of a loss of taxonomic identification accuracy among calanoid copepods in the ZooCAM dataset. Yet, this loss do not have a strong effect on the observed zooplankton community spatial patterns.

Imaging quality: illumination, imaging sensor, and image processing

Illumination, imaging sensor and image processing are potential causes of the significant differences in the abundances and biovolumes estimates of the transparent organisms such as Hydrozoans and Siphonophorae. Indeed, the latter had significantly higher abundances and biovolumes calculated with the ZooCAM than with the ZooScan. For example, the Siphonophorae biovolumes were estimated 16 and 60 times higher with ZooCAM than with the ZooScan for Sta. U0197 and U0256, respectively. Such differences may be explained by the instrument ability to image transparent objects, such as gelatinous organisms. The ZooScan illuminates objects from above with a white light planar illumination system (Gorsky et al. 2010) whereas the ZooCAM illuminates objects from the side using a flashing collimated red led (Colas et al. 2018). The ZooScan's sensor must be totally stable during the whole scanning process (3 min) to reach a good enough image sharpness while the flashing led coupled to the CCD ensure the sharpness of each individual image. The two instruments image processing steps are very similar although that of the ZooScan includes several image conversion steps (from 16-bits to 8-bits for example). Eventually, it appears that transparent objects are better imaged with

the ZooCAM than with the ZooScan. The edges and the transparent inner structures of the gelatinous zooplankton are more visible on the ZooCAM vignettes, enabling better detection, identification, count and a more precise size measurement. On the contrary, they appear lighter on the scans and the thresholding step of the image processing sometimes convert the lightest gray pixels into white pixels which are then no longer considered as a part of the object (Supporting Information Fig. S9). Consequently, the whole object is not always well detected and the following steps of identification and size measurement may be biased. Yet, our results show an overall good agreement between the two instruments suggesting that the illumination, sensors and image processing differences have a marginal effect on the outputs.

The benefits of comparing zooplankton imaging instruments

The comparison of the ZooScan and the ZooCAM highlights their interoperability on the large mesozooplankton size range, reflecting the possibility to combine zooplankton datasets originating from both instruments to expand their spatial and / or temporal coverage (e.g., Grandremy et al. 2023). Following this example, efforts should be made to inter-compare and inter-calibrate other imaging systems to evaluate their interoperability and therefore the possibility to assemble existing datasets in order to spatially and/or temporally extend zooplankton ecological studies. Also, inter-calibration and benchmarking of different imaging methods or instruments may enable to extend as well the size range of target organisms, paving the road toward more ecologically and biology integrated studies (e.g., Romagnan et al. 2015, who described the succession of whole plankton assemblages over time). Furthermore, benchmarking instruments would enable zooplankton time series initiated with an instrument to be completed and / or continued with another one in case of failure, obsolescence, or replacement. The continuation of times series, for zooplankton and for any other ecological variable is still critical in the current context of accelerating global changes. Another noteworthy remark is that expert zooplankton taxonomists are becoming increasingly rare, and zooplankton data increasingly expensive. Benchmarking traditional binocular examination with imaging instruments, and lab-based imaging instruments with live on-board or in situ instruments may help make cruise time more profitable and reduce the economic and environmental costs of land based lab analysis (sample processing, fixative use) therefore reducing the overall cost of zooplankton data collection. This would be achievable only by benchmarking instruments and methods. Our study highlighted another aspect of the usefulness of benchmarking imaging instruments and methods: instruments can be complementary and help get a better picture of the reality. This is highlighted by the Harosa and Siphonophorae that were better imaged with the ZooCAM methods and technique (live), and with the copepods for which the ZooScan enabled to better identify calanoids to the family level. Since the two instruments are inter-comparable, the two datasets could be combined to take into account their advantages, and mitigate the weaknesses of each of them. Finally, benchmarking instruments enables the detection of technical as well as methodological biases that could be overcome by developing instrumental, software or methodological upgrades, and could be addressed when developing new devices. Benchmarking studies such as the one presented here may help developers to design future instruments that would address known biases and would be interoperable with past and future instruments, ensuring the continuation of existing data series.

Data availability statement

The ZooScan data can be found in the SEANOE dataportal, in the dataset "PELGAS Bay of Biscay ZooScan zooplankton Dataset (2004-2016)" (doi: https://doi.org/10.17882/94052). The ZooCAM data can be found in the SEANOE dataportal, in the dataset "PELGAS Bay of Biscay ZooCAM zooplankton Dataset (2016-2019)" (doi: https://doi.org/10.17882/94040).

References

Ariza, A., J. C. Garijo, J. M. Landeira, F. Bordes, and S. Hernández-León. 2015. Migrant biomass and respiratory carbon flux by zooplankton and micronekton in the subtropical Northeast Atlantic Ocean (Canary Islands). Prog. Oceanogr. **134**: 330–342. doi:10.1016/j.pocean.2015.03.003

Banse, K. 1995. Zooplankton: Pivotal role in the control of ocean production: I. Biomass and production. ICES J. Mar. Sci. **52**: 265–277. doi:10.1016/1054-3139(95)80043-3

Batten, S. D., and others. 2019. A global plankton diversity monitoring program. Front. Mar. Sci. **6**: 321. doi:10.3389/fmars.2019.00321

Beaugrand, G., K. M. Brander, J. A. Lindley, S. Souissi, and P. C. Reid. 2003. Plankton effect on cod recruitment in the North Sea. Nature **426**: 661–664. doi:10.1038/nature02164

Beaugrand, G., and others. 2015. Synchronous marine pelagic regime shifts in the northern hemisphere. Philos. Trans. R. Soc. B **370**: 20130272. doi:10.1098/rstb.2013.0272

Beaulieu, S., M. M. Mullin, V. T. Tang, S. M. Pyne, A. L. King, and B. S. Twining. 1999. Using an optical plankton counter to determine the size distributions of preserved zooplankton samples. J. Plankton Res. **21**: 1939–1956. doi:10.1093/plankt/21.10.1939

Beers, J. R., and G. L. Stewart. 1970. The preservation of Acantharians in fixed plankton samples. Limnol. Oceanogr. **15**: 825–827. doi:10.4319/lo.1970.15.5.0825

Benfield, M., and others. 2007. RAPID: Research on automated plankton identification. Oceanography **20**: 172–187. doi:10.5670/oceanog.2007.63

Biard, T., and others. 2016. In situ imaging reveals the biomass of giant protists in the global ocean. Nature **532**: 504–507. doi:10.1038/nature17652

Chiba, S., S. Batten, C. S. Martin, S. Ivory, P. Miloslavich, and L. V. Weatherdon. 2018. Zooplankton monitoring to contribute towards addressing global biodiversity conservation challenges. J. Plankton Res. **40**: 509–518. doi:10.1093/plankt/fby030

Colas, F., and others. 2018. The ZooCAM, a new in-flow imaging system for fast onboard counting, sizing and classification of fish eggs and metazooplankton. Prog. Oceanogr. **166**: 54–65. doi:10.1016/j.pocean.2017.10.014

Culverhouse, P. F. 2015. Biological oceanography needs new tools to automate sample analysis. J. Mar. Biol. Aquacult. **1**: 1–2.

Culverhouse, P. F., N. Macleod, R. Williams, M. C. Benfield, R. M. Lopes, and M. Picheral. 2014. An empirical assessment of the consistency of taxonomic identifications. Mar. Biol. Res. **10**: 73–84. doi:10.1080/17451000.2013.810762

Doray, M., P. Petitgas, C. Saraux, and A.-S. Cornou. 2013. EchoR: R Package for computing indices of the state of fish population and communities, based on fisheries acoustic data, R Package. Ifremer.

Doray, M., and others. 2018. The PELGAS survey: Ship-based integrated monitoring of the Bay of Biscay pelagic ecosystem. Prog. Oceanogr. **166**: 15–29. doi:10.1016/j.pocean.2017.09.015

Gorsky, G., and others. 2010. Digital zooplankton image analysis using the ZooScan integrated system. J. Plankton Res. **32**: 285–303. doi:10.1093/plankt/fbp124

Grandremy, N., J.-B. Romagnan, C. Dupuy, M. Doray, M. Huret, and P. Petitgas. 2023. Hydrology and small pelagic fish drive the spatio–temporal dynamics of springtime zooplankton assemblages over the Bay of Biscay continental shelf. Prog. Oceanogr. **210**: 102949. doi:10.1016/j.pocean.2022.102949

Hays, G., A. Richardson, and C. Robinson. 2005. Climate change and marine plankton. Trends Ecol. Evol. **20**: 337–344. doi:10.1016/j.tree.2005.03.004

Hofmann, E. E. 2010. Plankton functional group models–An assessment. Prog. Oceanogr. **84**: 16–19. doi:10.1016/j.pocean.2009.09.002

Irisson, J.-O., S.-D. Ayata, D. J. Lindsay, L. Karp-Boss, and L. Stemmann. 2022. Machine learning for the study of plankton and marine snow from images. Ann. Rev. Mar. Sci. **14**: 277–301. doi:10.1146/annurev-marine-041921-013023

Jalabert, L., M. Picheral, C. Desnos, and A. Elineau. 2022. ZooScan Protocol. protocols.io. https://www.protocols.io/view/zooscan-protocol-bziyp4fw

Lombard, F., and others. 2019. Globally consistent quantitative observations of planktonic ecosystems. Front. Mar. Sci. **6**: 196. doi:10.3389/fmars.2019.00196

Luo, J. Y., J.-O. Irisson, B. Graham, C. Guigand, A. Sarafraz, C. Mader, and R. K. Cowen. 2018. Automated plankton image analysis using convolutional neural networks. Limnol. Oceanogr. Methods **16**: 814–827. doi:10.1002/lom3.10285

Mitra, A., and C. Davis. 2010. Defining the "to" in end-to-end models. Prog. Oceanogr. **84**: 39–42. doi:10.1016/j.pocean.2009.09.004

Naito, A., Y. Abe, K. Matsuno, B. Nishizawa, N. Kanna, S. Sugiyama, and A. Yamaguchi. 2019. Surface zooplankton size and taxonomic composition in Bowdoin Fjord, North-Western Greenland: A comparison of ZooScan, OPC and microscopic analyses. Polar Sci. **19**: 120–129. doi:10.1016/j.polar.2019.01.001

Nishikawa, J., and M. Terazaki. 1996. Tissue shrinkage of two gelatinous zooplankton, Thalia democratica and Dolioletta gegenbauri (Tunicata: Thaliacea) in preservative. Bull. Plankton Soc. Jpn. **43**: 1–7.

Omori, M. 1978. Some factors affecting on dry weight, organic weight and concentrations of carbon and nitrogen in freshly prepared and in preserved zooplankton. Int. Rev. Ges. Hydrobiol. Hydrogr. **63**: 261–269. doi:10.1002/iroh.19780630211

Orenstein, E. C., and others. 2022. Machine learning techniques to characterize functional traits of plankton from image data. Limnol Oceanogr **67**: 1647–1669. doi:10.1002/lno.12101

Petitgas, P., A. Goarant, J. Massé, and P. Bourriau. 2009. Combining acoustic and CUFES data for the quality control of fish-stock survey estimates. ICES J. Mar. Sci. **66**: 1384–1390. doi:10.1093/icesjms/fsp007

Petitgas, P., M. Doray, M. Huret, J. Massé, and M. Woillez. 2014. Modelling the variability in fish spatial distributions over time with empirical orthogonal functions: Anchovy in the Bay of Biscay. ICES J Mar Sci **71**: 2379–2389. doi:10.1093/icesjms/fsu111

Petitgas, P., M. Huret, C. Dupuy, J. Spitz, M. Authier, J. B. Romagnan, and M. Doray. 2018. Ecosystem spatial structure revealed by integrated survey data. Prog. Oceanogr. **166**: 189–198. doi:10.1016/j.pocean.2017.09.012

Picheral, M., S. Colin, and J. O. Irisson. 2017. EcoTaxa, a tool for the taxonomic classification of images. https://ecotaxa.obs-vlfr.fr/

Pitois, S. G., J. Tilbury, P. Bouch, H. Close, S. Barnett, and P. F. Culverhouse. 2018. Comparison of a cost-effective integrated plankton sampling and imaging instrument with traditional Systems for Mesozooplankton Sampling in the Celtic Sea. Front. Mar. Sci. **5**: 5. doi:10.3389/fmars.2018.00005

Platt, T., and K. Denman. 1978. The structure of pelagic marine ecosystems. J. Cons. Int. Explor. Mer. **173**: 60–65.

Romagnan, J.-B., and others. 2015. Comprehensive model of annual plankton succession based on the whole-plankton time series approach. PloS One **10**: e0119219. doi:10.1371/journal.pone.0119219

Romagnan, J. B., L. Aldamman, S. Gasparini, P. Nival, A. Aubert, J. L. Jamet, and L. Stemmann. 2016. High frequency mesozooplankton monitoring: Can imaging systems and automated sample analysis help us describe and interpret changes in zooplankton community composition and size structure - an example from a coastal site. J. Mar. Syst. **162**: 18–28. doi:10.1016/j.jmarsys.2016.03.013

Rubbens, P., and others. 2023. Machine learning in marine ecology: An overview of techniques and applications. ICES J. Mar. Sci. 1–25. doi:10.1093/icesjms/fsad100

Sieburth, J. M. N., V. Smetacek, and J. Lenz. 1978. Pelagic ecosystem structure: Heterotrophic compartments of the plankton and their relationship to plankton size fractions 1. Limnol. Oceanogr. **23**: 1256–1263. doi:10.4319/lo.1978.23.6.1256

Stukel, M. R., M. Décima, and M. R. Landry. 2022. Quantifying biological carbon pump pathways with a data-constrained mechanistic model ensemble approach. Biogeosciences **19**: 3595–3624. doi:10.5194/bg-19-3595-2022

Turner, J. T. 2015. Zooplankton fecal pellets, marine snow, phytodetritus and the ocean's biological pump. Prog. Oceanogr. **130**: 205–248. doi:10.1016/j.pocean.2014.08.005

UNESCO. 1968. Zooplankton Sampling: Review Papers of the Proceedings of the Symposium on the Hydrodynamics of Zooplankton Sampling., Monographs on Oceanographic methodology, 2. ISSN 0077-104X. Paris.

van der Lingen, C. D. 2002. Diet of sardine Sardinops sagax in the southern Benguela upwelling ecosystem. S. Afr. J. Mar. Sci. **24**: 301–316. doi:10.2989/025776102784528691

Vandromme, P., L. Stemmann, C. Garcìa-Comas, L. Berline, X. Sun, and G. Gorsky. 2012. Assessing biases in computing size spectra of automatically classified zooplankton from imaging systems: A case study with the ZooScan integrated system. Methods Oceanogr. **1–2**: 3–21. doi:10.1016/j.mio.2012.06.001

Whitmore, B. M., C. F. Nickels, and M. D. Ohman. 2019. A comparison between Zooglider and shipboard net and acoustic mesozooplankton sensing systems. J. Plankton Res. **41**: 521–533. doi:10.1093/plankt/fbz033

Zhou, M. 2006. What determines the slope of a plankton biomass spectrum? J. Plankton Res. **28**: 437–448. doi:10.1093/plankt/fbi119

Acknowledgments

NG acknowledges being funded by Region Pays de la Loire, FR, and Ifremer. The authors wish to thank the students, technicians, and scientists who participated in the zooplankton sampling and samples management on board and on land, and the crew of the R/V Thalassa involved in the PELGAS cruise in 2016.

Conflict of Interest

None declared.

Submitted 19 December 2022
Revised 18 August 2023
Accepted 07 September 2023

Associate editor: Paul F. Kemp